Journal of Simulation and Analysis of Novel Technologies in Mechanical Engineering
17 (4) (2025) 0087~0099
DOI 10.71939/jsme.2025.1220398

Research article

Numerical investigation of vertical and oblique impacts of coated projectiles on aluminum targets: focus on friction effects

Pooya Pirali[a*], Mohsen Heydari Beni[a], Amirhossein Alyaninejad[a], Jafar Eskandari Jam[a], Majid Eskandari Shahraki[b]

[a] *Faculty of Materials and Manufacturing Technologies, Malek Ashtar University of Technology, Tehran, Iran.*
[b] *Department of Aerospace Engineering, Faculty of Engineering, Ferdowsi University of Mashhad, Mashhad, Iran*

[*] ppirali@mut.ac.ir

(Manuscript Received --- 07 Oct. 2025; Revised --- 30 Dec. 2025; Accepted --- 02 Jan. 2026)

Abstract

This paper numerically investigates the ballistic performance of rigid and coated projectiles impacting aluminum targets, with an emphasis on the effect of friction between the projectile components and the target. Simulations were conducted using Abaqus/Explicit to model vertical and oblique impacts on aluminum targets with thicknesses of 25 and 76 mm. The results were validated against experimental data and analytical models. The findings indicate that in vertical impacts, increased friction between the coating and the target enhances residual velocity and penetration depth, while increased friction between the core and the coating reduces these parameters. In oblique impacts, higher friction leads to reduced penetration and an increased likelihood of ricochet. The results include residual velocities, penetration depths, crater diameters, and energy analyses, providing insights for optimizing anti-armor designs.

Keywords: Coated projectile, vertical impact, oblique impact, friction effects, aluminum targets, Abaqus simulation.

1- Introduction

The penetration of anti-armor (AP) projectiles into metallic targets is a critical and widely applied area in the field of ballistics, playing a significant role in the design and development of military and civilian armor [1]. These projectiles, due to their ability to penetrate hard and resistant materials, hold particular importance in defensive and offensive applications. Coated projectiles, consisting of a hard core (e.g., tungsten or hardened steel) and a soft coating (e.g., brass or copper), offer significant advantages over simple projectiles due to their unique characteristics, such as protecting the weapon barrel from wear and enhancing penetration performance in targets [2,3]. The coating of these projectiles interacts with the target surface during the initial stages of penetration, facilitating core separation through friction and deformation, which contributes to deeper penetration of the core into the target [4]. This feature enables coated projectiles to exhibit superior performance against metallic targets, such as aluminum or steel.

Previous studies have shown that multiple factors, including the target material, its thickness, the projectile's nose shape, initial

velocity, and impact angle, influence the penetration process and ballistic behavior [5,6]. In aluminum targets, particularly alloys like AL6061-T6, which are widely used in military and aerospace industries due to their lightweight and adequate strength, phenomena such as petalling (formation of metal petals at the penetration site) and plugging (detachment of a portion of the target) have been extensively observed [7,8].

These phenomena are highly dependent on the mechanical properties of the target and the impact conditions. However, the role of friction as a key parameter in the interaction between the projectile's coating and the target, or between the core and the coating, has received less attention [9]. Studies by Gupta et al. have focused on vertical and oblique impacts of projectiles on metallic targets, but comprehensive parametric analyses regarding the effect of friction in coated projectiles remain limited [1,10]. This gap in prior research highlights the need for a more detailed investigation of friction effects [11,12].

This study aims to address this research gap by numerically investigating the effects of friction on the ballistic performance of coated projectiles at an initial velocity of 742 m/s. Simulations conducted using Abaqus/Explicit software enable a detailed analysis of the projectile's behavior during vertical and oblique impacts on aluminum targets. The results of these simulations have been compared with experimental data and existing analytical models to ensure their accuracy and validity [12,13]. The primary objective of this research is to provide deeper insights into improving the design of anti-armor projectiles by fine-tuning the friction coefficients between the coating and the target and between the core and the coating. Such adjustments can optimize ballistic performance, enhance penetration or target destruction, and reduce the likelihood of ricochet at oblique impact angles [14,15].

In recent years, numerous studies have investigated projectile impact on targets under various numerical and experimental conditions, highlighting the importance of modeling parameters such as projectile–target interaction, contact models, and frictional conditions. For example, Cao and Fan [16] presented a numerical model for the penetration process of a deformable projectile into a metal plate, which more accurately captures the interaction between the projectile and the target. In addition, Wu et al. [17] analyzed penetration performance and residual velocity prediction in reactive powder concrete by integrating mesoscopic simulations with experimental tests. Other studies, such as the work by Tao et al. [18], examined projectile penetration into thin concrete targets at different impact angles, demonstrating the influence of impact direction on penetration outcomes. Furthermore, Mohammadi et al. [19] analyzed the dynamic behavior of nano-alumina–reinforced targets under projectile impact, providing guidance for improving target resistance. Moreover, Xiaodong et al. [20] investigated the penetration depth of projectiles into ultra-high-performance concrete targets through both simulations and experiments.

The findings of this study are expected to assist designers and engineers in developing advanced munitions and more resilient armor. The main novelty of this study lies in a comprehensive numerical investigation of friction effects in coated projectiles by independently considering coating–target and core–coating friction under both vertical and oblique impact conditions. The results reveal opposite roles of friction in

normal and oblique impacts and provide clear design guidelines for optimizing penetration performance and target damage.

2- Simulation modeling

Simulations were conducted using Abaqus/Explicit. Rigid projectiles (steel core) and coated projectiles (tungsten core with brass coating) were modeled. Aluminum targets with thicknesses of 25 and 76 mm and AL6061-T6 properties were considered. The Johnson-Cook model was applied for the target and coating [21]. Friction coefficients between the coating and target (0 to 0.4) and between the core and coating (0 to 0.3) were varied. Meshing was optimized with 0.5 mm elements at the impact site.

Two anti-armor projectiles with hard cores were used in this study, as shown in Fig. 1 One projectile has a steel core with a copper jacket, and the other has a tungsten core with a brass jacket. According to the laboratory tests reported in reference [22], no significant deformation was observed in the steel-core projectile; therefore, this projectile was modeled as a rigid and integral body. In addition, ballistic tests conducted with the tungsten-core projectile showed that its core remained unchanged compared to its pre-impact condition. Consequently, this projectile was modeled with a rigid core and a deformable jacket. In this study, the term rigid projectile refers to the steel-core projectile, while the term jacketed projectile refers to the tungsten-core projectile [22].

Fig. 1 Real images of the steel-core projectile (left) and the tungsten-core projectile (right) [22].

The length of the rigid projectile is 34.55 mm, its diameter is 7.84 mm, and its mass is 9.28 g. The exact dimensions of the projectile and the geometry modeled in the software are shown in Fig. 2. To reduce computational time and cost, and considering the symmetry of the projectiles and targets under normal (vertical) impact conditions, only one quarter of the geometries was modeled.

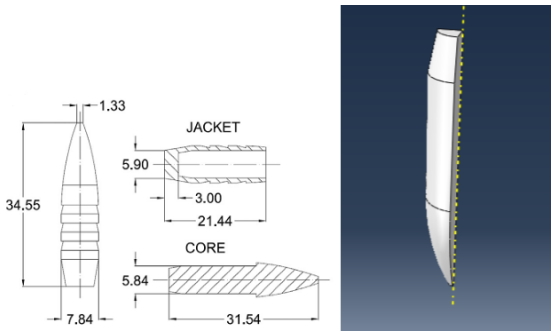

Fig. 2 Exact dimensions and the rigid projectile model used in the simulation [22].

The jacketed projectile has a conical-shaped core. The total mass of the projectile is 11.6 g, and the mass of the tungsten–carbide core is 5.1 g. The geometry and dimensions of the different parts of the projectile, as well as the modeled geometry of the jacket and core in the simulation, are shown in Fig. 3.

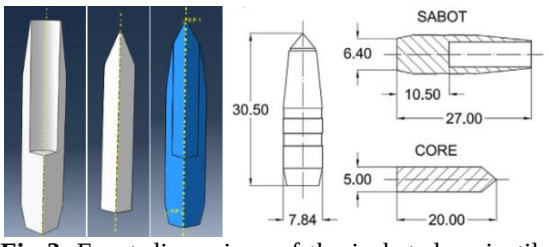

Fig 3. Exact dimensions of the jacketed projectile, showing the jacket and core separately and in the assembled configuration in the simulation [22].

The entire steel-core projectile was modeled as a rigid body; therefore, no material properties were assigned to it. Similarly, the core of the tungsten-core

projectile was modeled as rigid, while the brass jacket of the projectile, made of ZnCu30 alloy, was modeled as deformable. The Johnson–Cook material model was employed to define the strength and failure behavior of the jacket.

The target material was aluminum alloy Al6061-T6, and its physical and mechanical properties were extracted from reference [22] and assigned accordingly. The Johnson–Cook constitutive model was selected to simulate the strength behavior of the target material. To model the failure of the aluminum target, which is a relatively soft metal, the Bao–Wierzbicki fracture criterion was used.

An initial velocity condition V_0 was applied to both projectiles in the negative y-direction. Based on the experimental test observations reported in [22], initial velocities of 770 m/s and 742 m/s were assigned to the rigid projectile and the jacketed projectile, respectively.

For the 25-mm-thick target, residual stresses remained due to the rolling process applied during manufacturing. These stresses were incorporated into the simulation as initial pre-stresses. The residual stresses were applied to the target in both the rolling direction and the longitudinal direction. The magnitudes and locations of the applied residual stresses are shown in Figs. 4 and 5 [22].

According to the figures above, the stresses in the middle layer of the target are positive (tensile), while the stresses in the top and bottom layers of the target are negative (compressive). To apply boundary conditions to the targets, an encastre boundary condition was applied along the entire perimeter of the target so that it is fully constrained and cannot move at its edges.

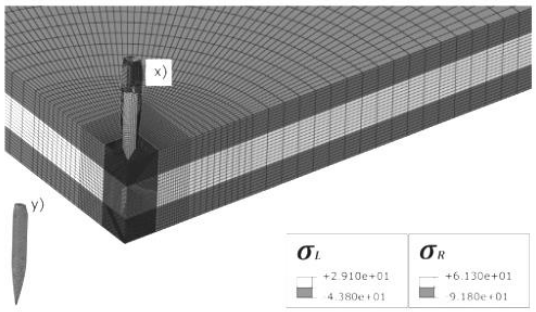

Fig. 4 Magnitude and location of residual stresses in the 25 mm target caused by the rolling process of the piece [22].

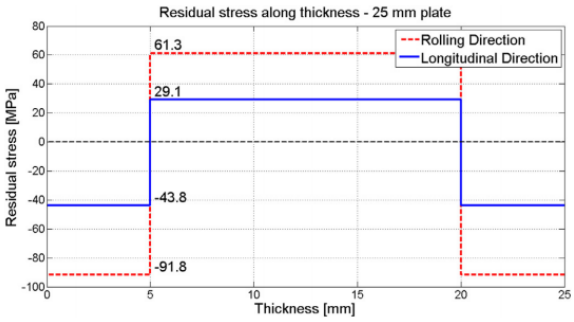

Fig. 5 Graph of residual stress values through the thickness of the 25 mm target resulting from the rolling process of the piece [22].

In the vertical impacts, since only one-quarter of the projectiles and targets were modeled, a symmetry boundary condition was applied to the cut surfaces of the projectile and the target. For the rigid projectile, since it is modeled as a single solid piece, only the contact between the projectile and the target was defined. Because the projectile penetrates the target and the target undergoes complete failure and destruction, surface contact alone is insufficient, and the definition of internal contact is required. The contact is of the general contact type, and for the rigid projectile, due to its solid nature, it is defined as frictionless.

For the jacketed projectile, in addition to defining internal contact between the core and the jacket with the target, contact between the projectile core and its jacket is also defined. This contact is of the surface-

to-surface type with a penalty feature, allowing the friction coefficients between the outer surfaces of the core and the inner surfaces of the jacket to be applied and adjusted.

In the present simulation, structured, Hexahedral, nonlinear elements were used. Figs. 6 and 7 show the final meshed models of the jacketed projectile and the 25 mm and 76 mm targets for vertical and oblique impacts.

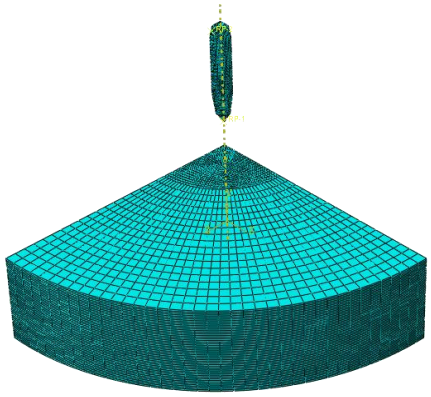

Fig. 6 Final meshed model for vertical impact of the jacketed projectile on the 25 mm target.

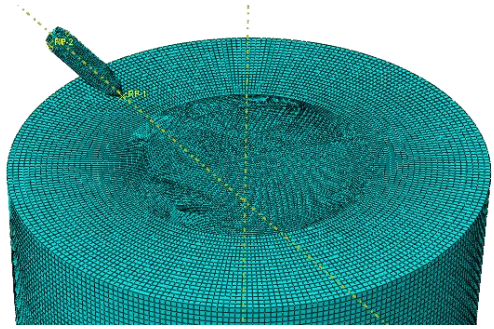

Fig. 7 Final meshed model for oblique impact of the jacketed projectile on the 76 mm target.

The residual velocity of the projectile after completely passing through the target, when a friction coefficient of 0.05 between the core and the jacket and 0.2 between the jacket and the target was considered, was obtained as 398 m/s. Considering that this value in reference [22] is 395 m/s, it differs by only 0.7% from the reference result. Based on the 395 m/s velocity reported in reference [22], it is concluded that an element size of 0.5 mm is the best choice for meshing in this project.

Table 1: Summary of mesh sensitivity results for the impact of the tungsten-core projectile on the 25 mm target.

Element Size (mm)	**1.5**	**1.0**	**0.75**	**0.5**	**0.3**
Residual Velocity (m/s)	196	283	325	398	Diverged Solution

3- Results

3.1 Vertical impacts

3.1.1 Effect of friction between coating and target

For the 25 mm target, increasing the friction coefficient between the coating and target (from 0.1 to 0.4) increased the residual velocity of the core from 391.8 to over 406.5 m/s, as the coating stopped earlier, facilitating core penetration (Table 2, Figure 8) [1,10]. For the 76 mm target, penetration depth varies from 32.3 to 35.5 mm (Table 3, Fig. 9) [7]. Figure 10 shows that with a friction coefficient of 0.4, the coating stopped at the target's initial surface, unlike the frictionless case [12]. Energy analysis indicates the conversion of kinetic energy to target strain energy [4,14].

Table 2: Residual velocity of tungsten core in coated projectile for 25 mm target with varying coating-target friction coefficients

Friction Coefficient	0	0.1	0.2	0.3	0.4
Residual Velocity (m/s)	512.5	391.8	396.8	401	406.5

Table 3: Penetration depth of tungsten core in coated projectile for 76 mm target with varying coating-target friction coefficients

Friction Coefficient	0	0.1	0.2	0.3	0.4
Penetration Depth (mm)	35.5	29	31.1	31.5	32.3

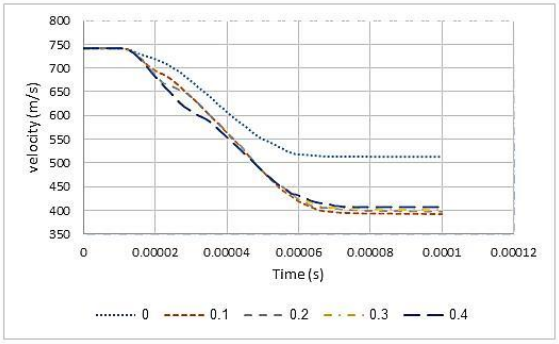

Fig. 8 Velocity-Time graph of the coated projectile with different friction coefficients for a 25 mm target.

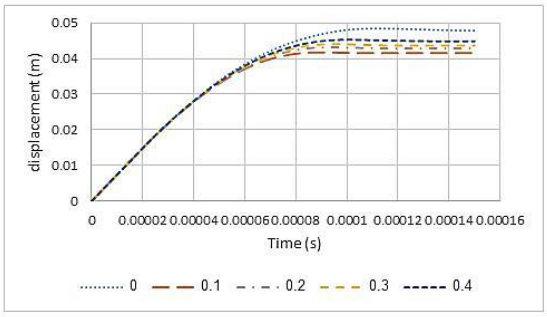

Fig. 9 Displacement-Time graph of the coated projectile core with different friction coefficients between the coating and the 76 mm target from the moment of launch to stoppage in the target.

Fig. 10 Penetration and damage mechanism of the tungsten-core coated projectile in a 76 mm target. the friction coefficient between the coating and the target is 0 in the top figure and 0.4 in the bottom figure.

3-1-2 Effect of friction between core and coating

Increasing the friction coefficient between the core and coating (from 0 to 0.3) reduced the residual velocity in the 25 mm target from 432 to 309 m/s (Table 4, Fig. 11) [3,9]. In the 76 mm target, the penetration depth decreased from 35.3 to 28.6 mm (Table 5, Fig. 12) [11]. With a friction coefficient of 0.05, separation of the core and coating occurred earlier (Fig. 13) [15].

Table 4: Residual velocities of tungsten core in coated projectile after passing through a 25 mm target with varying core-coating friction coefficients

Friction Coefficient	0	0.05	0.1	0.2	0.3
Residual Velocity (m/s)	432	398	385	339	309

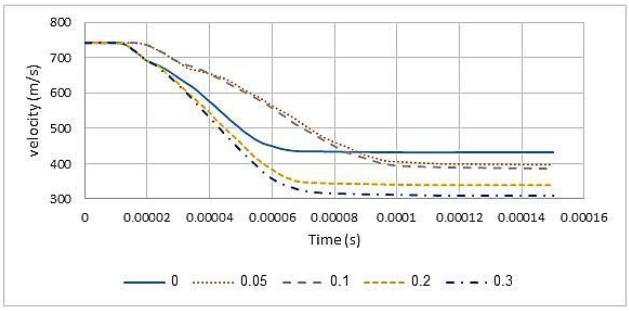

Fig. 11 Velocity-Time graph of the coated projectile core with different friction coefficients between the core and coating during impact on a 25 mm target.

Table 5: Penetration depth values of tungsten core in coated projectile for a 76 mm target with varying core-coating friction coefficients

Friction Coefficient	0	0.05	0.1	0.2	0.3
Penetration Depth (mm)	35.3	31.1	30.2	29.5	28.6

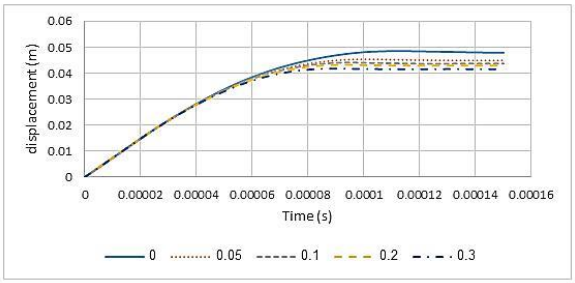

Fig. 12 Displacement-Time Graph of the Coated Projectile Core with Different Friction Coefficients Between the Core and Coating During Impact on a 76 mm Target.

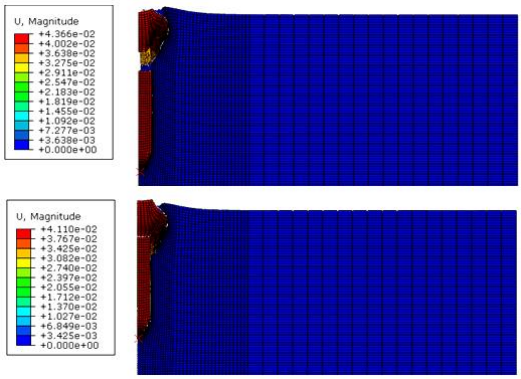

Fig. 13 Penetration Mechanism of the Tungsten-Core Projectile in a 76 mm Target Along with Displacement Contours. The Friction Coefficient Between the Core and Coating is 0.05 in the Top Figure and 0.3 in the Bottom Figure.

3-1-3 Crater entry and exit diameters

Increasing the friction coefficient between the coating and the target increased the crater diameters in both targets (Table 6, Fig. 14) [8,12]. The crater diameters in the simulations (10-15 mm) are consistent with experimental data [13]. The friction between the core and the coating had a negligible effect on the crater diameters (Table 7) [21].

3-2 Oblique impacts

3-2-1 Effect of friction between coating and target

For the 25 mm target, increasing the impact angle (30°, 45) and friction coefficient reduced the residual velocity from 462 m/s to 176 m/s (Table 8). Figures 15–17 show the kinetic energy graphs for impact angles of 30°, 45°, and 60° [1,5]. For the 76 mm target, penetration depth decreased from 41 mm to 10 mm (Table 9) [10]. At a 60° angle with zero friction, the coating ricocheted, but the core penetrated (Fig. 18) [12]. Energy analysis indicates the retention of kinetic energy at higher angles (Figs. 19–21) [4, 23].

Table 6: Entry and Exit Crater Diameters After Impact of Tungsten-Core Projectile on 25 mm and 76 mm Targets with Varying Coating-Target Friction Coefficients

Friction Coefficient	0	0.1	0.2	0.3	0.4
Entry Crater Diameter (mm) - 25 mm Target	12	9.7	10.2	10.4	10.5
Exit Crater Diameter (mm) - 25 mm Target	4.2	4.1	4.3	4.5	4.6
Entry Crater Diameter (mm) - 76 mm Target	10.3	10	10.5	10.7	10.8

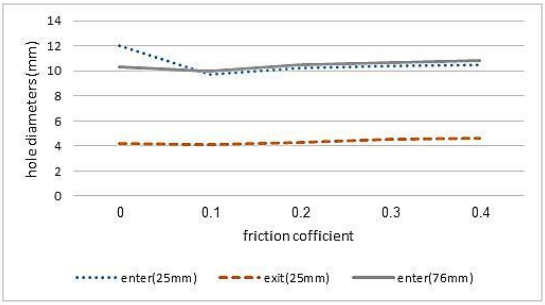

Fig. 14 Entry and Exit Crater Diameters Formed During the Impact of a Coated Projectile on 25 mm and 76 mm Targets.

Table 7: Entry and Exit Crater Diameters After Impact of Tungsten-Core Projectile on 25 mm and 76 mm Targets with Varying Core-Coating Friction Coefficients

Friction Coefficient (Core-Coating)	0	0.05	0.1	0.2	0.3
Entry Crater Diameter (mm) - 25 mm Target	10.4	10.2	10.2	10.1	10.1
Exit Crater Diameter (mm) - 25 mm Target	4.9	5.0	5.2	5.3	5.2
Entry Crater Diameter (mm) - 76 mm Target	9.5	9.5	9.5	9.7	9.6

Table 8: Residual Velocity Values of the Coated Projectile in Oblique Impacts on a 25 mm Target with Varying Coating-Target Friction Coefficients (m/s)

Friction Coefficient	30° Impact Angle	45° Impact Angle
0	462	340
0.1	371	252
0.2	360	212
0.3	352	199
0.4	348	176

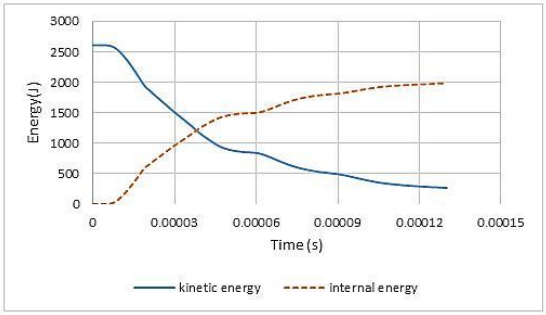

Fig. 15 Graph of Changes in Kinetic Energy of the Coated Projectile and Strain Energy of the Target Over Time During Oblique Impact on a 25 mm Target at a 30° Angle.

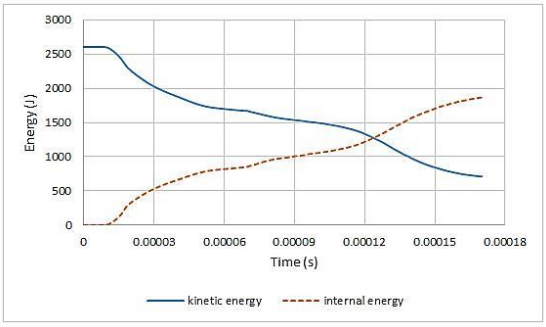

Fig. 16 Graph of Changes in Kinetic Energy of the Coated Projectile and Strain Energy of the Target Over Time During Oblique Impact on a 25 mm Target at a 45° Angle.

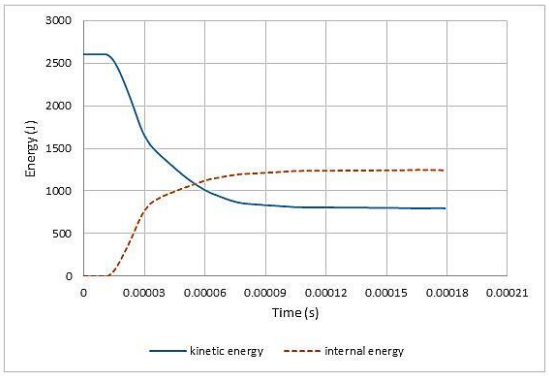

Fig. 17 Variation of the projectile's kinetic energy and the target's strain energy versus time in the oblique impact of a coated projectile on a 25-mm-thick target at an angle of 60 degrees.

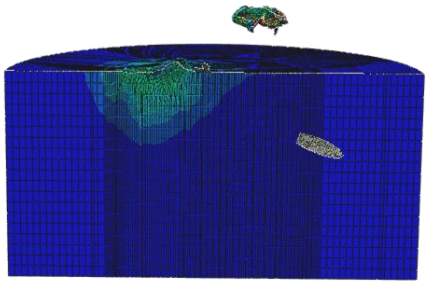

Fig. 18 Core penetration and coating ricochet in the oblique impact (60 degrees) of a coated projectile on a 76-mm-thick target in the case of no friction between the coating and the target.

Table 9: Values of the vertical penetration depth of the coated projectile in the oblique impact on a 76-mm-thick target with different friction coefficients between the coating and the target (values in millimeters).

Impact Angle (°)	Friction Coefficient 0	Friction Coefficient 0.1	Friction Coefficient 0.2	Friction Coefficient 0.3	Friction Coefficient 0.4
30	41	33.5	27.4	20.8	17
45	30	22.5	17.5	14.0	11.3
60	21 (coating ricochet)	12.5	10	stopped at target entry	stopped at target entry

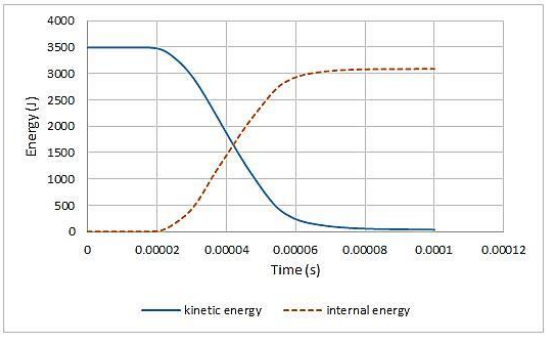

Fig. 19 Variation of the projectile's kinetic energy and the target's strain energy versus time in the oblique impact of a coated projectile on a 76-mm-thick target at an angle of 30 degrees.

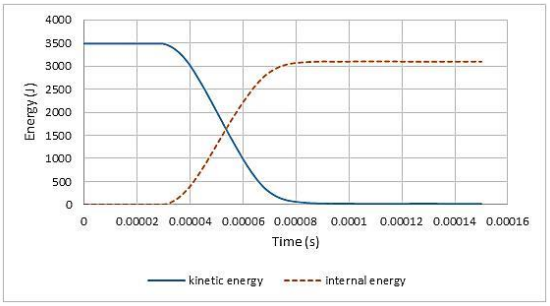

Fig. 20 Variation of the projectile's kinetic energy and the target's strain energy versus time in the oblique impact of a coated projectile on a 76-mm-thick target at an angle of 45 degrees.

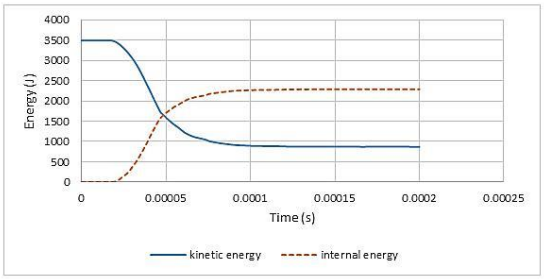

Fig. 21 Variation of the projectile's kinetic energy and the target's strain energy versus time in the oblique impact of a coated projectile on a 76-mm-thick target at an angle of 60 degrees.

3-2-2 Effect of friction between the core and the coating

Increasing the friction between the core and the coating reduced the residual velocity in the 25-mm target (Table 10, Figs. 22–24) [3,9]. In the 76-mm target, the penetration depth decreased (Table 11) [11]. At a 60° impact angle, the coating ricocheted (Fig. 25) [15]. Figure 26 shows the preservation of the coating's kinetic energy [14].

Table 10: Residual velocity values of the core in oblique impact on a 25-mm target with different friction coefficients between the projectile core and coating (m/s).

Impact Angle (°)	Friction Coefficient 0	Friction Coefficient 0.05	Friction Coefficient 0.1	Friction Coefficient 0.2	Friction Coefficient 0.3
30	625	360	347	320	308
45	530	212	204	191	180

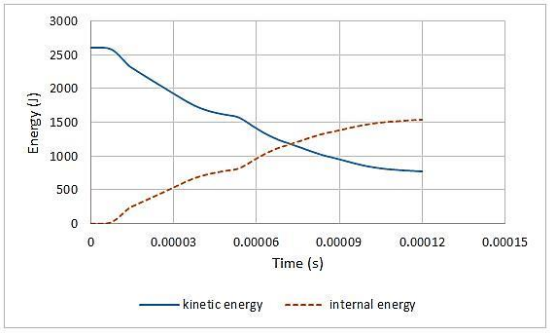

Fig. 22 Variation of the projectile's kinetic energy and the target's strain energy versus time in the oblique impact of a coated projectile on a 25-mm-thick target at an angle of 30 degrees.

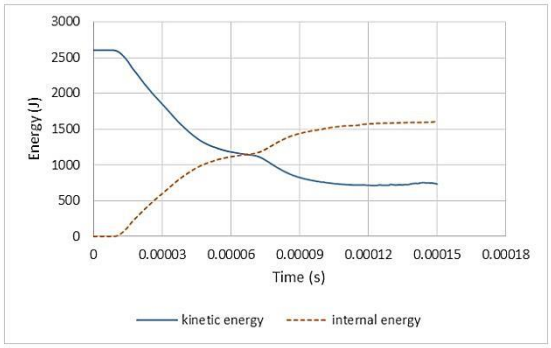

Fig. 23 Variation of the projectile's kinetic energy and the target's strain energy versus time in the oblique impact of a coated projectile on a 25-mm-thick target at an angle of 45 degrees.

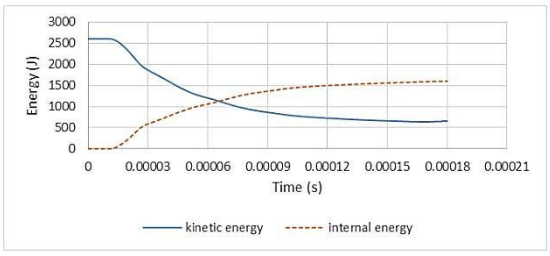

Fig. 24 Variation of the projectile's kinetic energy and the target's strain energy versus time in the oblique impact of a coated projectile on a 25-mm-thick target at an angle of 60 degrees.

Table 11: Vertical penetration depth values of the core in oblique impact on a 76-mm target with different friction coefficients between the projectile core and coating (values in millimeters).

Impact Angle (°)	Friction Coefficient 0	Friction Coefficient 0.05	Friction Coefficient 0.1	Friction Coefficient 0.2	Friction Coefficient 0.3
30	38	27.4	25	21.3	19.6
45	28.5	17.5	15.1	12.1	10
60	18.3	10	9.8	9.1	7.4

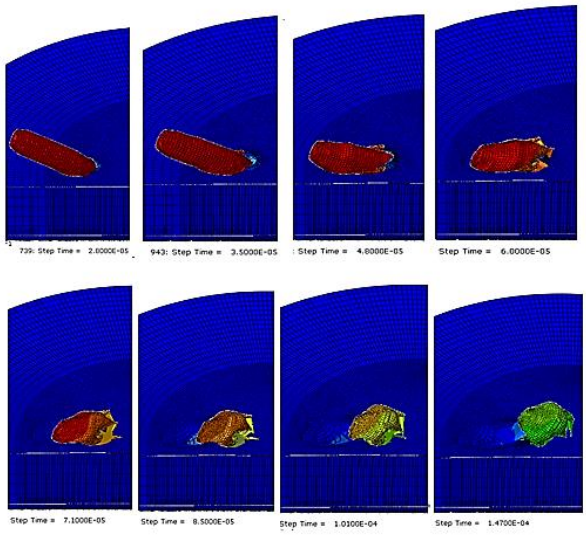

Fig. 25 Different stages of projectile penetration and coating separation and ricochet from the target in the oblique impact of a coated projectile on a 76-mm-thick target at an angle of 60 degrees.

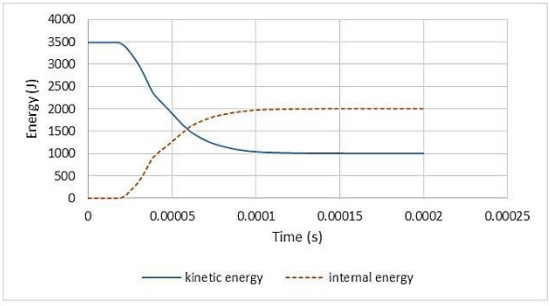

Fig. 26 Variation of the projectile's kinetic energy and the target's strain energy versus time in the oblique impact of a coated projectile on a 76-mm-thick target at an angle of 60 degrees.

3-2-3 Comparison of rigid and coated projectiles

The rigid projectile exhibited better performance (higher velocity and penetration), while the coated projectile caused greater damage (Table 12, Fig. 27) [2,12]. The energy transferred to the 25-mm target was higher with the coated projectile (Tables 13 and 14) [7,13].

Table 12: Comparison of the rigid and coated projectiles in impact on 25-mm and 76-mm targets.

Projectile Type	Residual Velocity after Passing through 25-mm Target (m/s)	Energy Absorbed by 25-mm Target (J)	Penetration Depth in 76-mm Target (mm)
Steel Core	525	1,454.83	47.44
Tungsten Core	400	2,792.88	35.5

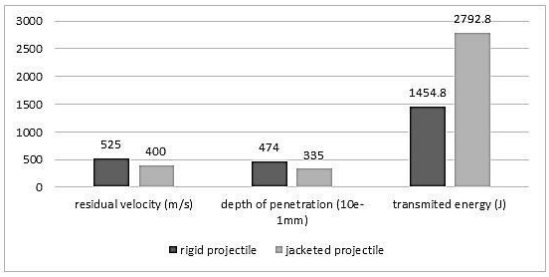

Fig. 27 Comparison of the rigid and coated projectiles in impact on 25-mm and 76-mm targets.

Table 13: Quantitative results of the coated projectile in vertical impact on 25-mm and 76-mm aluminum targets.

Variation of friction between coating and target (0.1 to 0.4)	The highest residual velocity of the core occurred at the highest friction coefficient, reaching **406.5 m/s**, which is a **3.75% increase** compared to a friction coefficient of 0.1.
	The greatest penetration depth of the core in the target occurred at the highest friction coefficient, reaching **32.3 mm**, an **11% increase** compared to friction 0.1.
	The largest entry hole diameter of the target occurred at the highest friction coefficient, reaching **10.8 mm**, an **8% increase** compared to friction 0.1.
	The largest exit hole diameter of the target occurred at the highest friction coefficient, reaching **4.6 mm**, a **12% increase** compared to friction 0.1.
Variation of friction between core and coating (0.05 to 0.3)	The highest residual velocity of the core occurred at the lowest friction coefficient, reaching **398 m/s**, which is a **29% increase** compared to friction 0.3.
	The greatest penetration depth of the core in the target occurred at the lowest friction coefficient, reaching **31.1 mm**, a **7.8% increase** compared to friction 0.3.
	The difference in hole diameters in this case was negligible; therefore, this friction has almost no effect on the hole diameters.

Table 14: Quantitative results of the coated projectile in oblique impact on 25-mm and 76-mm aluminum targets.

Change in Friction Coefficient Between Coating and Target from 0.1 to 0.4	The highest residual velocity of the core at a 30° angle corresponds to the lowest friction coefficient, measured at 371 m/s, representing a 6.6% increase compared to a friction coefficient of 0.4.
	The highest residual velocity of the core at a 45° angle corresponds to the lowest friction coefficient, measured at 252 m/s, representing a 31% increase compared to a friction coefficient of 0.4.
	The greatest penetration depth of the core in the target at a 30° angle corresponds to the lowest friction coefficient, measured at 35.5 mm, representing a 44% increase compared to a friction coefficient of 0.4.
	The greatest penetration depth of the core in the target at a 45° angle corresponds to the lowest friction coefficient, measured at 22 mm, representing a 48% increase compared to a friction coefficient of 0.4.
Change in Friction Coefficient Between Core and Coating from 0.05 to 0.3	The highest residual velocity of the core at a 30° angle corresponds to the lowest friction coefficient, measured at 360 m/s, representing a 16.8% increase compared to a friction coefficient of 0.3.
	The highest residual velocity of the core at a 45° angle corresponds to the lowest friction coefficient, measured at 212 m/s, representing a 17.7% increase compared to a friction coefficient of 0.3.
	The greatest penetration depth of the core in the target at a 30° angle corresponds to the lowest friction coefficient, measured at 27.4 mm, representing a 28% increase compared to a friction coefficient of 0.3.
	The greatest penetration depth of the core in the target at a 45° angle corresponds to the lowest friction coefficient, measured at 17.5 mm, representing a 42% increase compared to a friction coefficient of 0.3.

In Table 15, the results of the present simulation are compared with the simulation results and analytical model presented in reference [22], and the percentage errors are provided. As explained in previous sections, in this case, the friction coefficient between the projectile core and its jacket was considered as 0.05, and the friction between the brass jacket and the aluminum target was 0.2.

Given the very small differences between the two simulations, the accuracy of the simulations conducted in this study can be confirmed, ensuring the reliability of the results. The discrepancies are mainly due to the slight difference in element sizes between the two simulations: the smallest element size in the present simulation was 0.5 mm, whereas in the reference study it was 0.3 mm [22].

Table 15: Comparison of the present simulation results with the reference study [22] for the jacketed projectile.

Compared Parameters	Present Simulation	Reference Simulation	Reference Analytical Model	Percentage Error Relative to Reference Simulation
Residual velocity through 25 mm target (m/s)	398	395	379	0.7%
Penetration depth in 76 mm target (mm)	35.5	36.33	34.9	2%

4- Explanation of the trends in residual velocity and penetration depth

The variations in residual velocity and penetration depth of the projectile, as shown in the tables and figures, are directly influenced by the amount of energy dissipation and the manner in which kinetic energy is transferred between the projectile and the target. Increases or decreases in these parameters result from a complex interaction of resistive forces, including friction, plastic deformation of the target, and the core–jacket separation mechanism.

In vertical impacts, increasing the friction coefficient between the jacket and the target increases the shear force at the interface, causing the jacket to stop more quickly during the initial stages of penetration. This process concentrates kinetic energy in the

core, increases local pressure at the tip of the core, and consequently raises the residual velocity and penetration depth of the core into the target. Conversely, reducing the friction coefficient at this interface decreases energy transfer to the target and allows the jacket and core to move more synchronously, ultimately reducing the penetration effectiveness of the core.

On the other hand, increasing the friction coefficient between the core and the jacket increases energy transfer from the core to the jacket and raises internal energy dissipation within the projectile. By limiting the separation of the core from the jacket, this phenomenon reduces the residual velocity and penetration depth of the core in the target. In contrast, lower friction at this interface allows faster core separation, preserves its kinetic energy, and increases both residual velocity and penetration depth.

In oblique impacts, increasing the friction coefficient—either at the jacket–target interface or the core–jacket interface—enhances the resistant force component along the direction of motion, increases kinetic energy dissipation, and ultimately reduces residual velocity and penetration depth. This also raises the likelihood of jacket ricochet at larger impact angles.

Therefore, the trends observed in the tables and figures directly reflect the role of friction in energy distribution, projectile trajectory deviation, and penetration mechanisms under different impact conditions.

5- Conclusion

In vertical impacts of a coated projectile on soft targets with a constant friction coefficient between the core and the coating, increasing the friction coefficient between the coating and the target results in higher residual velocity and greater penetration depth of the projectile core in thin and thick targets, respectively.

In vertical impacts of a coated projectile on soft targets with a constant friction coefficient between the coating and the target, increasing the friction coefficient between the core and the coating leads to lower residual velocity and reduced penetration depth of the projectile core in thin and thick targets, respectively.

In oblique impacts of a coated projectile on soft targets with a constant friction coefficient between the core and the coating, increasing the friction coefficient between the coating and the target results in lower residual velocity and reduced penetration depth of the projectile core in thin and thick targets, respectively.

In oblique impacts of a coated projectile on soft targets with a constant friction coefficient between the coating and the target, increasing the friction coefficient between the coating and the target leads to lower residual velocity and reduced penetration depth of the projectile core in thin and thick targets, respectively.

In impacts of a coated projectile on soft targets with a constant friction coefficient between the core and the coating, increasing the friction coefficient between the coating and the target results in greater target destruction and larger entry and exit crater diameters.

For impacts of a coated projectile on soft targets, if the goal is to enhance ballistic performance parameters such as higher residual velocity and greater penetration depth, reducing the friction coefficient between the coating and the target is recommended. However, if greater target destruction is the priority, increasing the

friction coefficient between the coating and the target is suggested.

Reducing the friction coefficient between the core and the coating has no significant effect on target destruction but greatly influences the projectile's ballistic parameters. In all cases, reducing this friction coefficient is recommended in the design of coated projectiles.

References

[1] N.K. Gupta and V. Madhu, "Normal and oblique impact of a kinetic energy projectile on mild steel plates," *International Journal of Impact Engineering*, 12(3), 1992, pp. 333–343.

[2] H.F. Lehr, E. Wollman, G. Koerber, "Experiments with jacketed rods of high fineness ratio," *International Journal of Impact Engineering*, 17(4-6), 1995, pp. 517–526.

[3] A.A. Almohandes, M.S. Abdel-Kader, A.M. Eleiche, "Experimental investigation of the ballistic resistance of steel-fiberglass reinforced polyester laminated plates," *Journal of Composites Part B: Engineering*, 27(5), 1996, pp. 447–458.

[4] M.R. Edwards and A. Mathewson, "The ballistic properties of tool steel as a potential improvised armour plate," *International Journal of Impact Engineering*, 19(4), 1997, pp. 297–309.

[5] N.K. Gupta and V. Madhu, "An experimental study of normal and oblique impact of hard-core projectile on single and layered plates," *International Journal of Impact Engineering*, 19(5-6), 1997, pp. 395–414.

[6] Sorensen, B.R., et al., "Numerical analysis and modeling of jacketed rod penetration," *International Journal of Impact Engineering*, 22(1), 1999, pp. 71–91.

[7] Lee, M., "Analysis of jacketed rod penetration," *International Journal of Impact Engineering*, 24(9), 2000, pp. 891–905.

[8] Buyuk, M., et al., "Moving Beyond the Finite Element, a Comparison Between the Finite Element Methods and Meshless Methods for a Ballistic Impact Simulation," *8th International LS-DYNA Users Conference*, Detroit, 2004.

[9] Chocron, S., et al., "Impact of the 7.62mm APM2 projectile against the edge of a metallic target," *International Journal of Impact Engineering*, 25(5), 2001, pp. 423–437.

[10] Anderson, C.E., et al., "Numerical simulations of dynamic x-ray imaging experiments of 7.62-mm APM2 projectiles penetrating B4C," *19th International Symposium of Ballistics, Switzerland, 2001*.

[11] B.A. Pedersen, S.J. Bless, J.U. Cazamias, "Hypervelocity jacketed penetrators," *International Journal of Impact Engineering*, 26(1-10), 2001, pp. 603–611.

[12] Arild, T.J., "Numerical simulation of light armour piercing ammunition against steel," *FFI rapport*, 2005.

[13] Rosenberg, Z., et al., "Ricochet of 0.3" AP projectile from inclined polymeric plates," *International Journal of Impact Engineering*, 31(3), 2005, pp. 221–233.

[14] C. Roberson and P.J. Hazell, "Resistance of Silicon Carbide to Penetration by a Tungsten Carbide Cored Projectile," *Ceramic Transactions*, 151, 2003, pp.165-174.

[15] Nsiampa, N., et al., "Impact of 7.62 mm AP ammunition into aluminium 5083 plates," *23rd International Symposium on Ballistics*, Spain, 2007.

[16] S. Cao & J. Fan, Numerical model for penetration process of a deformable projectile into ductile metallic target plate considering the interaction of projectile and target. *International Journal of Impact Engineering*, 195, 2025, 105107.

[17] P. Wu, Y. Deng, C. Ma, Z. Wang, L. Li & Y. Zhang, Perforation performance study and residual velocity prediction of reactive powder concrete based on mesoscopic numerical simulation and experiments. *International Journal of Impact Engineering*, 210, 2026, 105596.

[18] Z. Tao, W. Li, W. Zhu, J. Xu & R. Ma, Experimental and numerical investigation of projectile penetration into thin concrete targets at an angle of attack. *Symmetry*, 17(11), 2025, 1904.

[19] S.F. Mohammadi, H. Ahmadi, E. Pedram, et al. Experimental tests and numerical analysis of the dynamic behavior of thin single and segmented nano-alumina-reinforced cementitious targets. *Archives of Civil and Mechanical Engineering*, 25, 2025, 139.

[20] I. Xiaodong, W. Xiangyun, L. Zhilin, Y. Zhi, J. Nan & G. Ruiqi, Research on penetration depth of projectiles into ultra-high performance concrete targets. *Explosion and Shock Waves*, 44(2), 2024, 023302.

[21] P.J. Hazell, C.J. Roberson, and M. Moutinho, "The design of mosaic armour: The influence of tile size on ballistic performance," *Materials and Design*, 29(8), 2008, pp. 1497–1503.

[22] Manes, A., et al. Perforation and penetration of aluminium target plates by armour piercing bullets. *International Journal of Impact Engineering*, 69, 2014. pp. 39 - 54.

[23] T. Børvik, S. Dey, and A.H. Clausen, "Perforation resistance of five different high-strength steel plates subjected to small-arms projectiles," *International Journal of Impact Engineering*, 36(7), 2009, pp. 948–964.